Shortening the heat treatment of third generation advanced high strength steels by forming carbide free bainite in the presence of martensite

Avila, Daniel dos S.; van Bohemen, Stefan M.C.; Huizenga, Richard M.; Offerman, S. Erik; Santofimia, Maria J.

DOI
10.1016/j.msea.2025.148241

Publication date
2025

Document Version
Final published version

Published in
Materials Science and Engineering: A

Materials Science & Engineering A 931 (2025) 148241

Contents lists available at ScienceDirect

Materials Science & Engineering A

journal homepage: www.elsevier.com/locate/msea

Shortening the heat treatment of third generation advanced high strength steels by forming carbide free bainite in the presence of martensite

Daniel dos S. Avila [a,*], Stefan M.C. van Bohemen [b], Richard M. Huizenga [a], S. Erik Offerman [a], Maria J. Santofimia [a]

[a] Department of Materials Science and Engineering, Delft University of Technology, Mekelweg 2, 2628 CD, Delft, the Netherlands
[b] Tata Steel, IJmuiden, the Netherlands

ARTICLE INFO

Keywords:
Advanced high strength steels
Carbide free bainite
Sheet steels
Quenching and partitioning

ABSTRACT

Successful implementation of third generation advanced high strength steels (3rd gen AHSS) can be accelerated by developing steels that can be heat treated in existing industrial lines. Here, we develop new carbide free bainitic (CFB) steels in which bainite formation is accelerated by a 0.2 volume fraction of prior martensite and thus can be realized in 5 min, making them suitable for manufacturing in modern continuous annealing lines for bare steel strips. The resulting microstructure consists of bainitic ferrite, tempered martensite, and retained austenite. Carbon and silicon had the most pronounced effect on the mechanical properties among the studied alloying elements (manganese, niobium, chromium, and molybdenum) because of their influence on the fraction and stability of retained austenite. Our proposed treatment, which we call bainite accelerated by martensite (BAM), showed higher strength and lower global formability than traditional CFB without prior martensite (also called TRIP-assisted bainitic ferrite, TBF) and quenched and partitioned (Q&P) steels. Five of the designed steels showed tensile strength higher than 1370 MPa, a total elongation higher than 8%, and hole expansion capacity higher than 30%, and thus meet the requirements for the strongest commercial grades of complex phase steels with improved formability. This work broadens the possibilities of using existing industrial lines for manufacturing novel 3rd gen AHSS.

1. Introduction

The pressure on the automotive industry to simultaneously decrease car weight and increase passenger safety has stimulated the quick development of novel high strength sheet steels in the past 30 years, such as the so-called advanced high strength steels (AHSS) [1]. The first generation (1st gen) of AHSS achieved higher ultimate tensile strength (UTS) than the then-available commercial steels, although with limited ductility (e.g. 5% total elongation at 1180 MPa ultimate tensile strength – UTS – for a complex-phase grade [2]). The balance of strength and ductility came by combining a soft ferrite matrix with hard martensitic or bainitic regions and, in some cases, regions of retained austenite. The family of 1st gen AHSS includes dual phase (DP) [3], transformation induced plasticity aided (TRIP) [4], and complex phase (CP) [5] steels.

As there is still a large pressure to reduce carbon emissions in the automotive industry by reducing car weight, the combination of strength and ductility achievable in 1st gen AHSS is not sufficient for current and future demands. Highly alloyed austenitic steels exhibiting twinning induced plasticity (TWIP) achieve a much higher combination of ductility and strength (e.g. 70% total elongation at 1200 MPa of UTS [6]). These alloys were called 2nd gen AHSS. However, the elevated cost associated with high alloying restricted the widespread industrial application of such steels [1].

A 3rd generation of AHSS started being developed in the late 2000s with the goal of achieving better strength-ductility balance than the 1st gen AHSS but with much lower alloying than 2nd gen AHSS. The improved mechanical properties with respect to 1st gen AHSS were achieved by avoiding or drastically reducing ferrite formation and introducing a larger fraction of retained austenite. Prominent members of the third generation of AHSS family are carbide-free bainitic (CFB) [7] – also called TRIP-assisted bainitic ferrite, TBF – and quenched and partitioned (Q&P) [8] steels. Medium manganese steels, which are also members of the 3rd gen AHSS family, still have a significant ferrite fraction, such as in 1st gen AHSS, but have a large fraction of

* Corresponding author.
E-mail address: D.dosSantosAvila@tudelft.nl (D.S. Avila).

https://doi.org/10.1016/j.msea.2025.148241
Received 13 November 2024; Received in revised form 18 March 2025; Accepted 18 March 2025
Available online 19 March 2025

manganese-enriched retained austenite [9].

Despite 3rd gen AHSS being intensively researched since 2005, their global commercialization started only after 2015 [10,11]. One of the reasons for this delay is that, despite such steels having lower alloying content than 2nd gen AHSS, the necessary heat treatment could not be directly performed in existing industrial lines dedicated to 1st gen AHSS [12]. The general treatment of Q&P steels is two-step, which involves quenching to a temperature T_q, which controls the martensite fraction, and reheating to a temperature T_p for carbon diffusion and partitioning [13–15]. It is possible to achieve mechanical properties suitable for 3rd gen AHSS with a one-step Q&P (T_p equal to T_q), which does not require reheating, but, at low T_p, carbon may not sufficiently homogenize in the remaining austenite [16]. Therefore, the alloy design should be tuned to avoid the formation of fresh martensite during cooling to room temperature, as fresh martensite can compromise the local formability of the steel.

TBF steels adopt a heat treatment comparable to 1st gen TRIP steels, with the main difference being that in TBF steels, bainite is formed after full austenitization, while in 1st gen TRIP, steels bainite is formed after intercritical annealing. To achieve sufficient hardenability and avoid ferrite formation, the alloying content in TBF steels is higher than in 1st gen TRIP steels, which in turn slows down the kinetics of bainite formation, rendering it too long to be used in some industrial lines. In continuous annealing lines for bare cold-rolled steels, bainite formation happens in the overaging section and is restricted to a maximum of 600 s for 2 mm thickness strips and 360 s for 1 mm thickness strips [1]. However, in many recently developed TBF steels with mechanical properties compatible with 3rd gen AHSS, the required time for bainite formation is between 7 and 90 min [17–24]. Short times (below 7 min) were tested in the works of Sugimoto et al. [7,25–29] and Ebner et al. [30]. Despite being restricted to such short times, Sugimoto et al. achieved a 1370 MPa tensile strength with 30% hole expansion capacity (HEC) – which is a measure of local formability [31] – and 8% total elongation [28]. Such results, which were the best combination of strength and formability, were achieved for a single condition out of 50 tested combinations of different niobium contents and isothermal holding temperatures. Moreover, the isothermal holding temperature that led to these specific mechanical properties was 100 °C below the martensite start temperature (M_S), and hence the majority phase was tempered martensite – not bainite.

In the present work, we study the influence of alloying elements (C, Si, Mn, Cr, Mo, and Nb) on the microstructure, kinetics, and mechanical properties of 3rd gen advanced high strength sheet steels designed to be manufactured in continuous annealing lines. A careful balance between the elements is needed because the alloying should be high enough to ensure sufficient hardenability and avoid ferrite formation but lean enough so that bainite can be formed in the overaging section of existing modern continuous annealing lines. To help achieve this balance, we form bainite at around 20 °C below M_S in the presence of around 0.2 volume fraction of prior martensite to take advantage of the martensite-induced bainite acceleration [32]. We benchmark such a heat treatment, called here bainite accelerated by martensite (BAM), against conventional TBF and two-step Q&P heat treatments. The proposed material and heat treatment achieves a UTS of 1420 MPa, a total elongation of 9%, and a HEC of 30% after isothermal bainite formation for 300 s. Such properties meet the requirements of the new steel grade CR1000Y1370T-CH, which is the strongest complex phase steel with improved formability in VDA's (German Association of the Automotive Industry) recent standard for 3rd gen AHSS [33], while having a heat treatment suitable for modern continuous annealing lines.

2. Experimental procedure

Steel ingots with eight different chemical compositions (Table 1) and 25 kg each were manufactured at Tata Steel (IJmuiden, The Netherlands) using a vacuum induction melting furnace. The compositions were selected to allow the study of the effects of C, Mn, Si, Cr, Mo, and Nb content. The ingots were reheated to 1230 °C, annealed for 45 min, and rough milled from 100 to 40 mm thick. Each roughed ingot was cut into 70 mm long blocks and each block was reheated to 1230 °C for 30 min and hot rolled in five steps from 40 to 3.8 mm thick. Hot rolling started at 1170 °C and finished at 900 °C. The hot rolled slabs were transported to a Run-Out-Table simulator in which slabs were cooled with a cooling rate of 30–40 °C/s to arrive at a coiling temperature of about 630 °C. The slabs were put in the furnace, and a standard coiling simulation program was applied. The coiling temperature of 630 °C and slow furnace cooling ensure that a ferrite-pearlite microstructure is formed in the hot rolled slabs. Finally, the pickled slabs were cold rolled to a final thickness of 1 mm and cut to appropriate sizes for dilatometry and annealing in a continuous annealing simulator (CASim).

Phase fractions (retained austenite, tempered martensite, fresh martensite, and bainite) and the kinetics of bainite formation were measured using dilatometry and X-ray diffraction (XRD). A Bähr 805 A/T dilatometer was used in quench mode with quartz rods, He-flow cooling, and 10 × 5 × 1 mm^3 samples cut from the cold rolled sheets, with the long direction of the sample parallel to the rolling direction. One thermocouple was spot-welded at the center of the sample, which was used for temperature control, and one spot-welded 1 mm from the border of the sample, which was used to measure the thermal gradient at the sample [34]. XRD experiments were performed in a Bruker D8 Advance diffractometer in a Bragg-Bretano geometry with graphite monochromator and Vantec position-sensitive detector using Co Kα radiation and operating at 40 kV and 40 mA with a divergence slit V4. The step size was 0.035° (2θ), and the counting time per step was 3 s.

Samples of selected steels were heat treated in the dilatometer, according to the thermal profiles of Fig. 1a, to measure the fraction of austenite decomposed as a function of temperature during cooling and of time during isothermal holding. The phase fractions were calculated using the lever rule with the nonlinear coefficients of thermal expansion of iron [35]. The distance between the expansion curves for austenite and martensite/bainite was adjusted to match the fraction of retained austenite at room temperature measured by XRD. The same procedure

Table 1
Chemical composition of the steels tested and relevant temperatures of the heat treatment in the CASim. Ref is the reference composition, and all other steels are named based on the change in their composition with respect to the reference material. M_S is the martensite start temperature, with an estimated error of ±10 °C, and the meaning of the other temperatures is found in the heat treatment scheme in Fig. 1b.

Steel	Chemical composition (wt.%)						Temperature (°C)					
	C	Mn	Si	Cr	Mo	Nb	M_S	T_{aus}	T_{TBF}	T_{BAM}	T_Q	T_P
Ref	0.240	2.28	1.51	–	–	–	359	900	390	340	280	400
0.6Si	0.246	2.26	0.61	–	–	–	355	840	390	340	280	400
1.0Si	0.246	2.34	1.05	–	–	–	370	865	390	340	280	400
0.02Nb	0.241	2.31	1.55	–	–	0.026	370	900	390	340	280	400
1.7Mn-0.6Cr	0.241	1.68	1.54	0.59	–	–	374	910	390	350	290	400
1.7Mn-0.6Cr-0.2Mo	0.234	1.73	1.56	0.59	0.18	–	370	910	390	350	290	400
0.27C-1.7Mn-0.6Cr	0.273	1.73	1.49	0.59	–	–	351	900	390	330	270	400
0.30C-1.7Mn-0.6Cr	0.304	1.71	1.46	0.58	–	–	330	890	390	310	250	400

was applied in previous works [36]. The fraction of retained austenite was measured from the XRD experiments following the procedure of Jatczak [37]. Three body-centered cubic (BCC) peaks – {110}, {200}, and {211} – and four face-centered cubic (FCC) peaks – {111}, {200}, {220}, and {311} – were integrated using xrdfit [38].

To analyze the mechanical properties, the cold rolled sheets were heat treated in a continuous annealing simulator (CASim) according to the heat treatments shown in Fig. 1b, which are named BAM (bainite accelerated by martensite), TBF (TRIP-assisted bainitic ferrite), and Q&P (quenched and partitioned). BAM also stands for the initials of the expected phases: bainite, austenite, and martensite. In the CASim, the extremities of the steel sheet (550 mm in length and 100 mm in width) are clamped by metallic grips, and the heat treatment is applied by Joule heating. Two sheets were made for each combination of steel and heat treatment. Two JIS5 tensile samples [39] were cut from one of the sheets, and two HEC samples (90 × 90 mm^2) were cut from the other sheet. After tensile testing, one 10 × 10 × 1 mm^3 sample was cut from the head of the specimen, which was undeformed, and one was cut from the deformed part of the specimen, close to – but not including – the neck. The cross-sections normal to the transversal direction of such samples were ground and polished, using the same procedure used for microstructural characterization described in the following paragraph, and analyzed in the XRD to measure the fraction of retained austenite.

Microstructural characterization was carried out in the scanning electron microscopes (SEM) JEOL JSM-6500F and Thermo Fisher Helios G4 UXe PFIB. Samples were cut from the head of the tensile test specimens, and the cross-section normal to the transversal direction was analyzed. All samples were ground up to 2000 mesh silicon carbide grinding paper, polished up to 1 μm diamond suspension, and etched with Nital 2 %.

The pair of JIS5 longitudinal direction (L) tensile test pieces machined from each annealed CASim sheet were tested according to ISO 6892-1-2016 using a 250 kN Zwick-Roell AllroundLine materials testing machine with a laserXtens contactless extensometer. The average values of tensile properties including yield strength (YS), ultimate tensile strength (UTS), total elongation (TE) are reported.

The hole expansion capacity (HEC) tests were performed according to ISO 16630. A 10 mm diameter hole was punched in each HEC sample of 90 mm × 90 mm with a flat punch and 12% clearance. The HEC tests were performed burr upwards with a conical punch (60° apex angle). The hole expansion capacity, also known as the hole expansion ratio (HER), was calculated as $100(d - d_0)/d_0$, with $d_0 = 10$ mm, and d the diameter recorded when the first crack over the strip thickness occurred.

3. Results

3.1. Kinetics of bainite formation

Fig. 2 shows the kinetics of bainite formation for the reference steel and steel 0.6Si. Based on the dilatometry cooling curves, no austenite decomposition into ferrite or bainite took place during cooling from austenitization to the isothermal holding temperature. In the reference steel, which is alloyed with 1.5Si, the transformation reaches stasis before austenite is fully decomposed. The bainite fraction formed at stasis increases with decreasing temperature. This phenomenon, referred to as incomplete reaction, is common in steels alloyed with silicon. Silicon retards cementite formation, and carbon which is in excess of the carbon solubility in bainitic ferrite is partitioned to the austenite. The driving force for bainite nucleation and growth decreases as austenite is enriched with carbon, until the point at which bainite cannot form anymore. The carbon content in austenite at stasis can be calculated either using the T_0 or T_0' temperatures, which assume the diffusionless theory of bainite formation [40], or using the WB_s temperature, which assumes the diffusional theory [41]. Both theories indicate that the lower the temperature the higher the carbon content in austenite at stasis and the higher the fraction of bainite at stasis.

The austenite remaining after bainite formation in the reference steel can transform to martensite upon cooling to room temperature. Fig. 2b shows the change in length during the final cooling for the different isothermal temperatures tested. The volume fraction of martensite formed during cooling, calculated from the lever rule, was 0.26 for isothermal holding at 455 °C, 0.08 for isothermal holding at 415 °C, and less than 0.05 for all other temperatures. The fraction of martensite formed during cooling decreases with isothermal holding temperature because the remaining austenite is more enriched in carbon after bainite formation at lower temperatures (based on the T_0' and WB_S temperatures) and, consequently, its martensite start temperature is lower [42].

Fig. 2a shows that the kinetics of bainite formation is accelerated by decreasing the isothermal holding temperature in steel Ref even without the presence of prior martensite. This effect is because of the incomplete

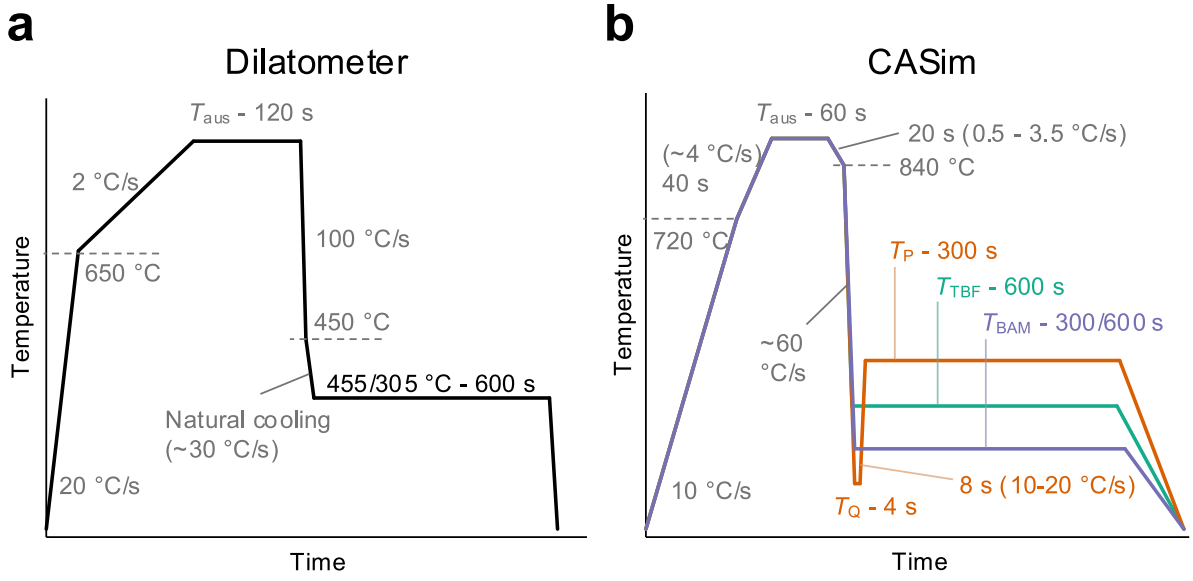

Fig. 1. Heat treatments applied in (a) the dilatometer and (b) in the CASIM. Natural cooling was used in the dilatometer for isothermal treatments below 450 °C to minimize the thermal gradients in the sample [34]. T_{aus}, T_Q, T_P, T_{TBF}, and T_{BAM} for the CASim are given for each steel in Table 1. T_{aus} for the dilatometer is similar to T_{aus} for the CASim, unless otherwise stated.

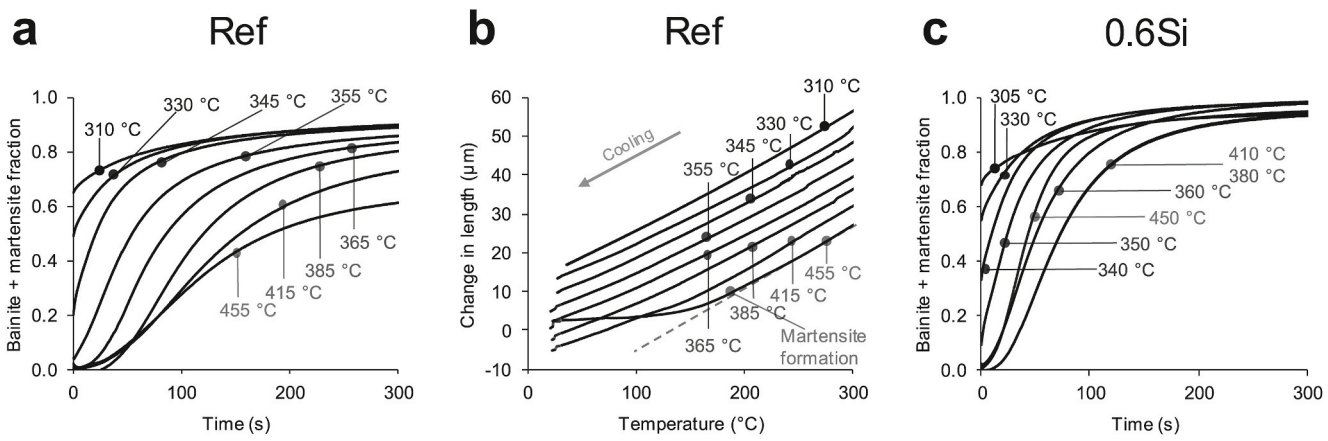

Fig. 2. Kinetics of bainite formation at different isothermal temperatures for steel (a) Ref and (c) 0.6Si; and (b) change in length during cooling after bainite formation for steel Ref, in which a deviation from the nonlinear expansion coefficient indicates the formation of martensite. T_{aus} was 925 °C for steel Ref and 875 °C for steel 0.6Si. The raw data is available in the linked dataset [60].

transformation, as less bainite is formed at higher temperatures. For steel 0.6Si, which almost fully transforms to bainite at any given temperature, the kinetics of bainite formation slows down when the temperature is decreased from 450 °C down to 380 °C, as Fig. 2c shows. The opposite trend to steel Ref strongly indicates that the incomplete reaction phenomenon played a strong role in accelerating bainite formation at lower temperatures for steel Ref. The results in Fig. 2 indicate that the partitioning of carbon to austenite slowed down the kinetics of bainite formation, especially at higher temperatures, as the formation of bainite is faster for steel 0.6Si than for steel Ref. Consequently, for steel 0.6Si, the transformation to bainite was complete within 300 s even when no prior martensite was formed.

In Steel 0.6Si, from 360 °C and below, some martensite is formed prior to bainite formation, and the kinetics of bainite formation is accelerated. Despite 360 °C being 5 °C above M_S for steel 0.6Si, there was an undershoot in the temperature during cooling – especially in the border of the sample, which was in contact with the cold dilatometer rods –, and a volume fraction of 0.02–0.05 of martensite was formed. Such a low fraction is already efficient in accelerating bainite formation. At 350 °C, with a prior martensite fraction of 0.09, bainite formation is faster than at 450 °C. Such results confirm that the effect of bainite acceleration by the presence of prior martensite operates in these steels.

The curves of bainite formation for steels Ref and 0.6Si were presented here to illustrate the bainite-accelerating effect induced by prior martensite. All other compositions were also tested, and a similar accelerating effect was observed for all steels.

3.2. Microstructure

Fig. 3 shows the microstructure of the different steels after being treated in the CASim. The microstructures consist of bainitic ferrite, films of retained austenite, martensite/austenite (MA) islands, and, for the heat treatments BAM and Q&P, tempered martensite. Some carbides may be present, especially in the steel 0.6Si. The fraction of retained austenite measured by XRD is presented in Fig. 4. No proeutectoid ferrite was observed in any of the samples. Based on the visual analysis of the micrographs, and on the model developed by van Bohemen and Morsdorf [43], the prior austenite grain size of all steels is estimated to be in the order of 10 µm.

The reference steel showed large MA islands after the TBF treatment. After the BAM treatment, the MA islands are smaller and more dispersed. Such MA islands are formed from the austenite remaining after the end of the isothermal holding step. This remaining austenite partly transforms to martensite upon cooling to room temperature. In the BAM treatment, bainite formation is faster, and the fraction of remaining austenite is lower than in the TBF (Fig. 2a), which contributes to having fewer and smaller islands of remaining austenite.

The size of MA islands in the Q&P treatment was similar to those in TBF for the reference steel. Such MA islands are formed from the austenite remaining after quenching to T_Q that did not decompose into bainite during partitioning at T_P. The martensite fraction formed upon quenching to T_Q was estimated to be 0.80, and the volume fraction of retained austenite was measured as 0.14 by XRD. Thus, most of the austenite remaining after quenching to T_Q does not decompose into bainite during partitioning and is retained at room temperature.

In steel 0.6Si, the low silicon content resulted in less retained austenite, as shown in Fig. 4, and possibly more carbide formation. However, a few MA islands were still found in steel 0.6Si, as can be observed in Fig. 3. Such MA islands mostly lie in bands parallel to the rolling direction and are probably in regions with pronounced chemical segregation of alloying elements, such as manganese. These regions are formed during the solidification of the steel ingots.

The addition of 0.026 wt% Nb changed the morphology of the MA islands and of the films of retained austenite. In the reference steel with the TBF treatment, there were thin, elongated films of retained austenite, and the MA islands were large and blocky. Conversely, in steel 0.02Nb, there were significantly fewer films of retained austenite, and the MA islands were smaller and globular.

The mechanism by which niobium changed the morphology of the MA islands and the films of retained austenite is not clear. One possibility is that the presence of niobium carbides induces the intragranular nucleation of bainite at the carbide/austenite interface. According to Thermo-Calc equilibrium simulations using the database TCFE12 [44], 98 % of the niobium atoms are in undissolved NbC carbides at the austenitization temperature (900 °C). Additionally, niobium strongly segregates to austenite grain boundaries and hinders grain growth [45]. Therefore, the change in morphology could also be caused by the change in prior austenite grain size or by a change in the nucleation rate of bainite at austenite grain boundaries caused by the higher niobium content at such boundaries. However, no clear difference in prior austenite grain size induced by the addition of niobium could be observed in the micrographs shown in Fig. 3 and in the supplementary materials.

The substitution of 0.6 wt% Mn for 0.6 wt.% Cr in steel 1.7Mn-0.6Cr refined the MA islands in the TBF treatment, possibly due to faster kinetics of bainite formation, as Fig. 5 shows. In the BAM treatment, a few large regions with carbide precipitation inside were present, as indicated in Fig. 3. Such areas are typical of tempered martensite [46] formed slightly below M_S [47].

Increasing the carbon content from 0.24 to 0.30 led to a lower

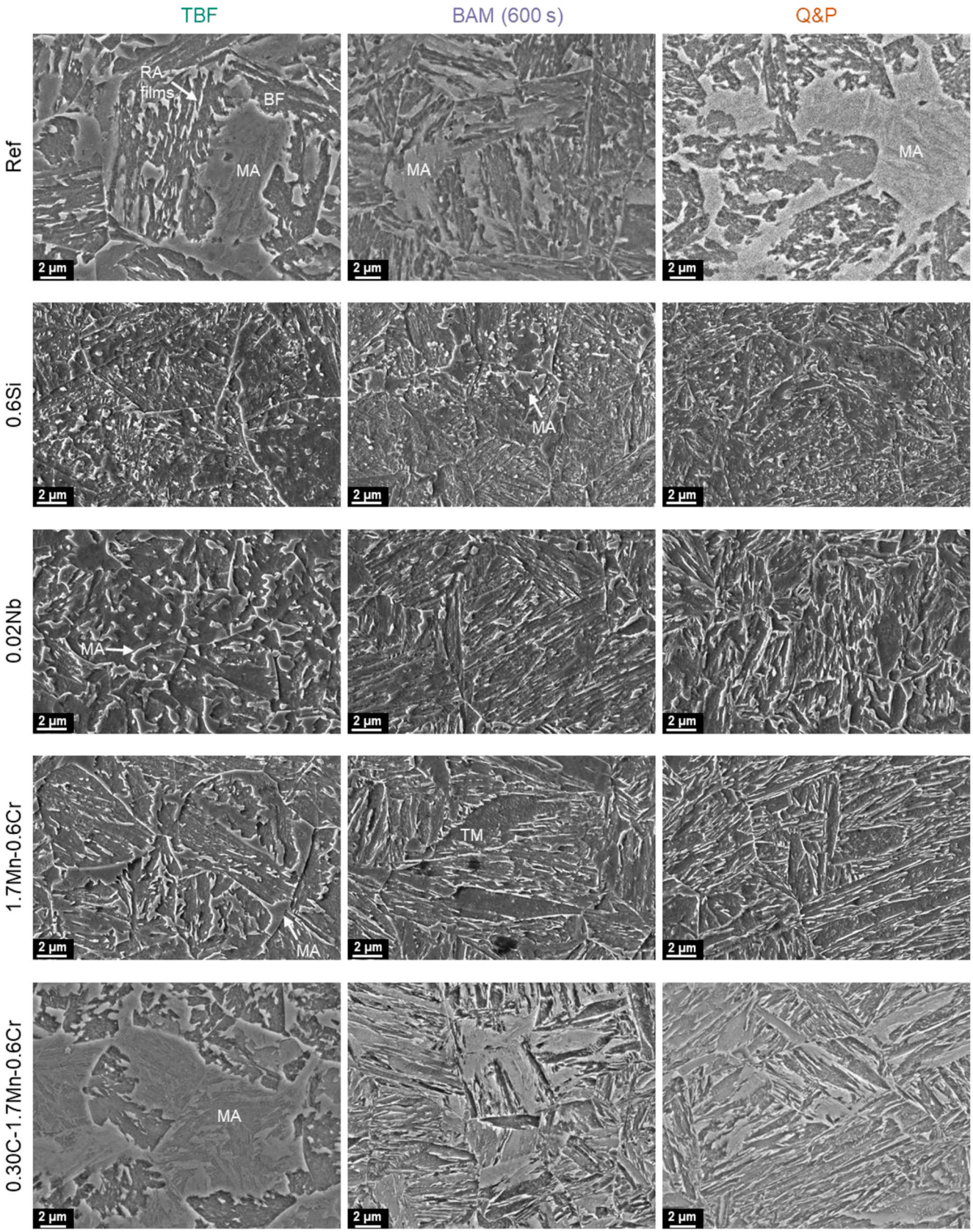

Fig. 3. Microstructure of samples treated in the CASim. Rows indicate the steel and columns indicate the heat treatment. Annotations indicate bainitic ferrite (BF), tempered martensite (TM), islands of martensite and austenite (MA), and films of retained austenite (RA). Images were acquired in the SEM and the samples were etched with Nital 2 %. The isothermal holding time for the BAM samples was 600 s. Extra micrographs, including from the conditions not shown here, are available in the linked dataset.

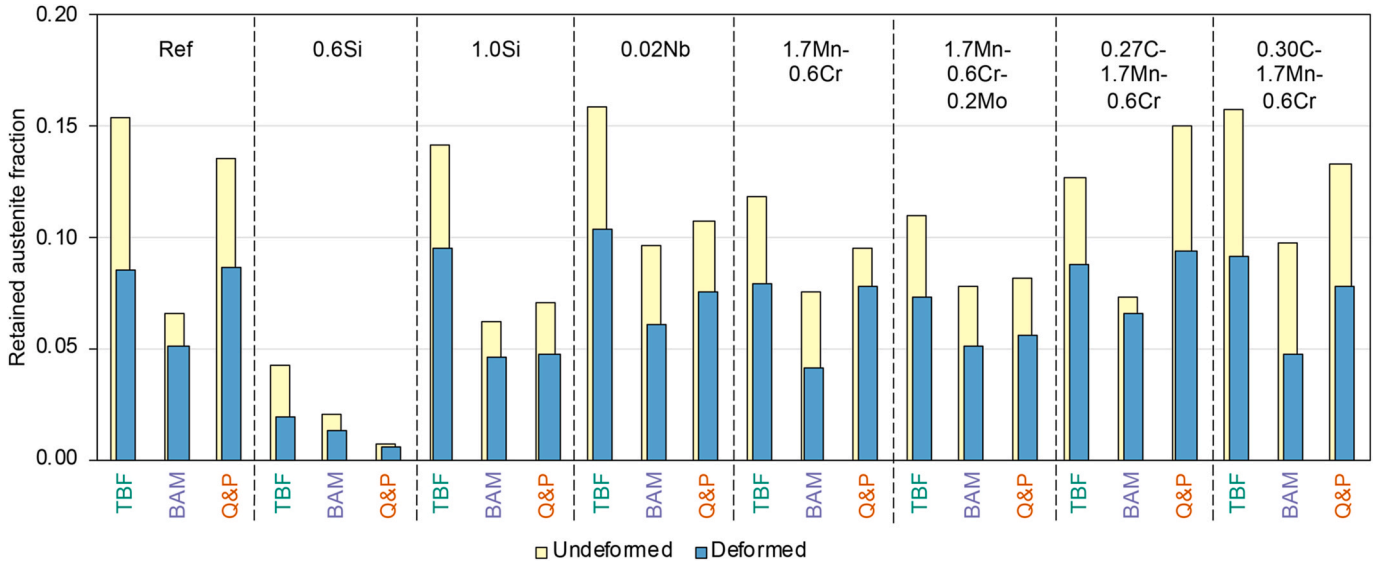

Fig. 4. Volume fraction of retained austenite measured in the specimens for tensile testing in the undeformed and in the deformed region of the specimens. The isothermal holding time for the BAM samples was 600 s. The reduced fraction in the deformed regions indicates that austenite transformed to martensite during tensile testing. The absolute uncertainty of the measured fractions is largely influenced by the texture resulting from cold rolling [48], which could not be estimated because it would require multiple experiments. However, as the production and rolling parameters of all steels were the same and the XRD patterns were taken from the same orientation in all samples, the uncertainty in the difference in the austenite fraction between steels should be much smaller (around 0.01–0.02 [49]). The raw data is available in the linked dataset [60].

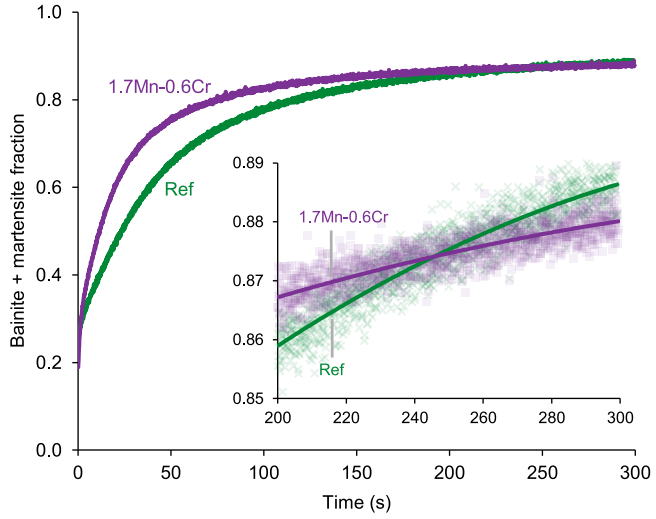

Fig. 5. Kinetics of bainite formation in the presence of martensite for steel Ref and 1.7Mn-0.6Cr. T_{aus} was 850 °C for steel Ref and 860 °C for 1.7Mn-0.6Cr, and the holding time at T_{aus} was 60 s. Isothermal bainite formation was for 300 s at 340 °C for steel Ref and 350 °C for steel 1.7Mn-0.6Cr. For both steels, the volume fraction of prior martensite was around 0.25. Inset shows the final 100 s of isothermal holding.

fraction of bainite formation in the TBF and BAM treatments. This is indicated by the apparent increase in the number and size MA islands, seen in Fig. 3, and can also be inferred by the theoretical maximum value of bainite calculated from the $T_0^{'}$ and WB_S, both of which indicate increasing the carbon content decreases the fraction of bainite formed at stasis. Despite the increased number and size of MA islands in steel 0.30C-1.7Mn-0.6Cr, its fraction of retained austenite is comparable to steel Ref, 0.02Nb, and 1.7Mn-0.6Cr, which indicates that in steel 0.30C-1.7Mn-0.6Cr there is more fresh martensite.

3.3. Mechanical properties

Fig. 6 shows the plot of the total elongation (TE), which is a measurement of the global formability, and of the hole expansion capacity (HEC), which is a measurement of the local formability, against the ultimate tensile strength (UTS) of the steels annealed in the CASim. The highest UTS was achieved by the BAM steels, followed by the Q&P and the TBF steels. The trend for total elongation was the opposite, with the TBF steels having the highest elongation, followed by the Q&P and the BAM steels. The highest HEC was achieved by the Q&P steels, followed by the BAM and the TBF steels. Table 2 presents the average mechanical properties of all chemical compositions, grouped by heat treatment, also including the BAM treatment with 300 s of isothermal holding time. The mechanical properties for each individual combination of steel and heat treatment are shown in Table A1, in Appendix A.

The reduction in the isothermal holding time from 600 s to 300 s for the BAM steels resulted only in a slight change in mechanical properties. This change is small because, given the accelerating effect of martensite, bainite formation is close to stasis after 300 s of isothermal holding (see kinetics of bainite formation for Ref steel at 345 °C in Fig. 2).

From an industrial and commercial point of view, the mechanical properties achieved can be benchmarked against the recently approved VDA standard 239-100, which includes requirements for complex and dual phase steels with improved formability (CH and DH, respectively). Despite the different naming, CH and DH grades can be considered to encompass TBF and Q&P steels [11,50]. The stronger grade in these families is called CR1000Y1370T-CH, with YS between 1000 and 1250 MPa, UTS between 1370 and 1550 MPa, and total elongation above 5%. Including an extra requirement of HEC >30 %, to ensure sufficient local formability, five steels with the BAM 300 s treatment meet these specifications and deliver a surplus in total elongation, which goes up to 9%: Ref, 0.6Si, 1.0Si, 1.7Mn-0.6Cr, and 1.7Mn-0.6Cr-0.2Mo.

4. Discussion

4.1. Effect of the heat treatment

The macroscopic mechanical properties depend on the mechanical

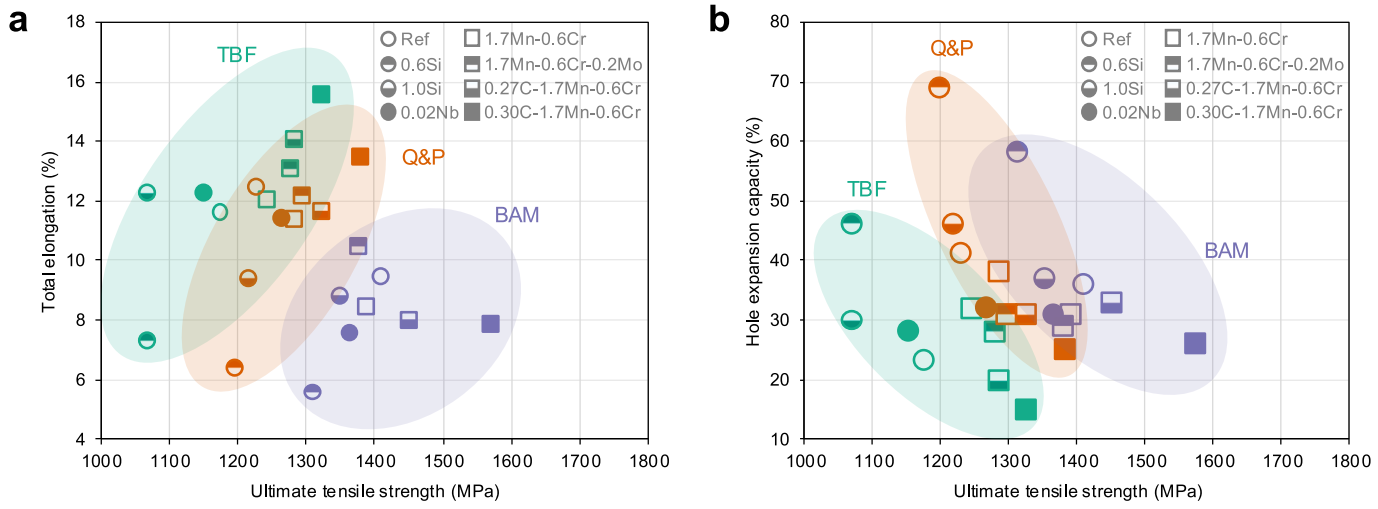

Fig. 6. Ultimate tensile strength vs (a) total elongation and (b) hole expansion capacity of all steels treated in the CASim. Shape of the markers indicates the chemical composition, and the color indicates the heat treatment. The isothermal holding time for the BAM samples was 600 s. (For interpretation of the references to color in this figure legend, the reader is referred to the Web version of this article.)

Table 2
Mechanical properties of the steels heat treated in the CASim for each heat treatment. Values are the average and standard deviation for each group, with each heat treatment group including the eight chemical compositions from Table 1.

Heat treatment	YS (MPa)	UTS (MPa)	TE (%)	HEC (%)
BAM (600 s)	1083 ± 18	1405 ± 79	8 ± 1	35 ± 10
BAM (300 s)	1023 ± 55	1451 ± 102	9 ± 1	30 ± 8
TBF	854 ± 54	1201 ± 98	12 ± 2	28 ± 9
Q&P	1116 ± 36	1276 ± 60	11 ± 2	39 ± 14

properties of the individual phases that constitute the steel's microstructure, and on how these different microstructural constituents interact. A simple yet reasonably accurate assumption is that the strength is given by the average of the individual strength of the microstructure constituents – retained austenite, bainite, tempered martensite, and fresh martensite, in the present case – weighted by their volume fraction [17].

BAM steels achieved 200 MPa higher UTS and YS than TBF steels. In both groups of steels, bainite constitutes the major phase (70–90%) and is thus expected to be the most important microstructure constituent controlling the strength. While bainite was formed at 390 °C for all TBF steels, it was formed at 310–350 °C in BAM steels. Bainite formed at lower temperatures is finer and, consequently, stronger. The thickness of bainite plates can be estimated as a function of temperature as [51].

$$u_T = 0.2\frac{(T-528)}{150}, \quad (1)$$

where u_T is the thickness in μm and T is the temperature in kelvin. The strengthening contribution from the size of bainite plates is estimated as [52].

$$\sigma_T = \frac{115}{2u_T}, \quad (2)$$

where σ_T is the strengthening contribution in MPa.

From Eq. (1), the average thickness of bainite plates is 0.180 μm at 390 °C (average TBF temperature) and 0.111 μm at 338 °C (average BAM temperature). From Eq. (2), the size contribution to the strength of bainite is 319 MPa for TBF and 519 MPa for BAM. The 200 MPa increase in strength predicted for bainite is consistent with the experimental measurements summarized in Table 2: On average, UTS increased by 200 MPa and YS increased by 230 MPa from TBF to BAM with 600 s isothermal holding. Fig. 7 shows the change in UTS and YS for individual steels, and such a strengthening was seen in all cases. The increase in UTS varied from 102 MPa (1.7Mn-0.6Cr-0.2Mo) to 284 MPa (1.0Si), and the increase in YS varied from 150 MPa (1.7Mn-0.6Cr-0.2Mo) to 330 MPa (0.30C-1.7Mn-0.6Cr).

The contribution of solid solution and precipitate (such as fine carbides) strengthening is expected to be the same in both groups. Additionally, the initial dislocation density is expected to be higher for BAM samples as bainite formed at lower temperatures displays a higher dislocation density [52], which further strengthens bainite. However, it is hard to quantitatively assess the effect of the higher initial dislocation density in the yield strength because yield may start first in retained austenite.

The higher strength for BAM compared to TBF reported here contrasts with the work of Navarro-López et al. [18], who reported the same UTS for BAM and TBF. However, in their work, a higher fraction of fresh martensite (~0.12) was formed for TBF than for BAM (~0.03–0.05). Such fresh martensite is formed from the carbon-enriched austenite and hence is expected to be much stronger than the bainitic ferrite or the tempered martensite. Conversely, in the present work only a low fraction of fresh martensite (<0.05) is formed after both TBF and BAM treatments.

Retained austenite is a minority phase, with a volume fraction of up to 0.16. However, thanks to the TRIP effect, it can have a pronounced effect on the global formability of steels. The XRD results presented in Fig. 4 show that the fraction of retained austenite is, on average, 33% lower in the deformed regions of the tensile specimen than in the undeformed regions. This result confirms that part of the austenite transformed into martensite during deformation, which indicates that the TRIP effect took place.

In Fig. 8a, the volume fraction of retained austenite is plotted against the total elongation for all steels. There is a positive correlation between the fraction of retained austenite and the total elongation, which is because of the TRIP effect, as indicated by the results from XRD. Steels that underwent the BAM heat treatment have a lower austenite fraction than TBF and Q&P, which is possibly the reason for their limited elongation. Fig. 7 shows that, for all steels, the TBF heat treatment resulted in higher total elongation than the BAM treatment. The chemical and mechanical stability of retained austenite are also important factors controlling TRIP effect, and differences in carbon content, morphology

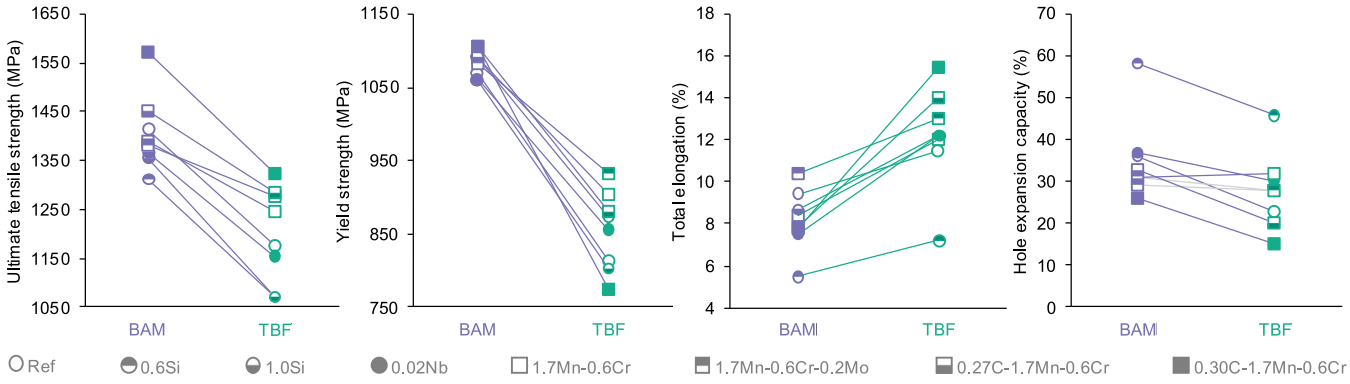

Fig. 7. Mechanical properties of BAM steels with 600 s isothermal holding time compared to TBF steels.

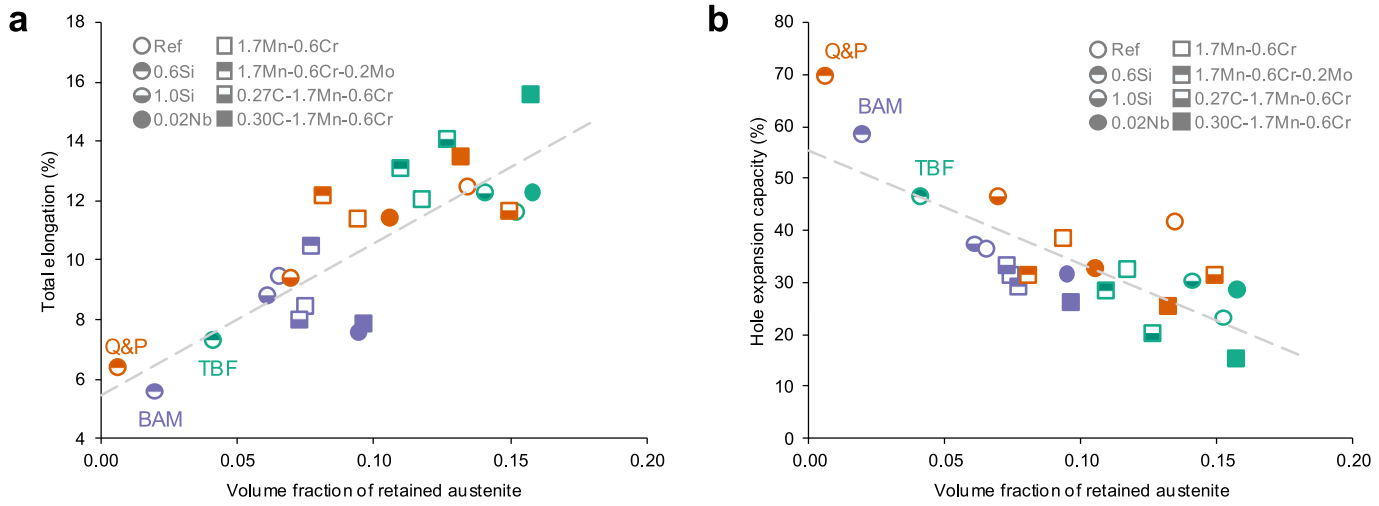

Fig. 8. Volume fraction of retained austenite plotted against (a) total elongation and (b) hole expansion capacity. Shape of the markers indicates the chemical composition, color indicates the treatment, and dashed line is the linear trend. The isothermal holding time for the BAM samples was 600 s. (For interpretation of the references to color in this figure legend, the reader is referred to the Web version of this article.)

of retained austenite, and different residual stresses may explain the scatter in Fig. 8.

The transformation of austenite to martensite during deformation can have a positive effect on global formability, as deduced from the increase in total elongation. However, it can also have a negative impact on local formability, as indicated by the lower hole expansion capacity. Martensite formed from the carbon-enriched retained austenite is much harder than other microstructure features because of its high carbon content; large differences in hardness between microstructure features are harmful to local formability [31]. Fig. 8b shows that there is a negative correlation between the fraction of retained austenite and the hole expansion capacity.

Compared to TBF, BAM has a lower fraction of retained austenite and, in turn, presents slightly higher HEC (Fig. 7). However, Q&P showed a higher HEC than BAM, despite the Q&P having more retained austenite. A possible reason for this result is the carbon heterogeneity in austenite. The partitioning step for Q&P took place at 400 °C, while bainite formation for BAM took place at temperatures ranging from 310 to 350 °C, and hence carbon distribution in austenite might be more homogeneous in Q&P than in BAM steels. Under strain, austenite with heterogenous carbon distribution will generate martensite with a gradient in hardness – which negatively impacts HEC [53]. Also, any region of retained austenite that is relatively poor on carbon could readily transform to martensite even under low stress. A different origin for the higher HEC for Q&P steels could be the effect of martensite tempering. During partitioning, the martensite formed during the initial quench is tempered. If the mechanical properties of the strongly tempered martensite in Q&P steels are more homogeneous in comparison to the mixture of softly tempered martensite and carbide free bainite in the BAM samples, this leads to an improved HEC.

The ratio between the YS and UTS, called yield ratio (YR), has been shown to correlate with the HEC. Kim et al. [53] gathered data on the YR and HEC from different families of steels (DP, Q&P, TRIP, TWIP, martensitic, and medium manganese) and found a linear trend between YR and HEC. Fig. 9a shows the YR plotted against HEC for the steels developed in the present study. Although we also found a linear trend between YR and HEC, as did Kim et al., a single linear trend did not fit well all data points. Instead, grouping steels by heat treatment and calculating the linear trend separately for each group results in a more accurate trend. This result shows that even though YR correlates with HEC, this correlation is more accurate when used to compare steels with similar microstructures that underwent similar heat treatments. Fig. 9b shows the relation between YR and the fraction of retained austenite. In this case, the linear trends for the BAM and TBF groups match well, but the trend for Q&P is best described by its own linear trend.

4.2. *Effect of chemical composition*

In Fig. 6, the mechanical properties for all chemical compositions and three different heat treatments were shown. The chemical compositions of the steels differ from each other in their content of silicon, carbon, manganese, chromium, molybdenum, and niobium (Table 1).

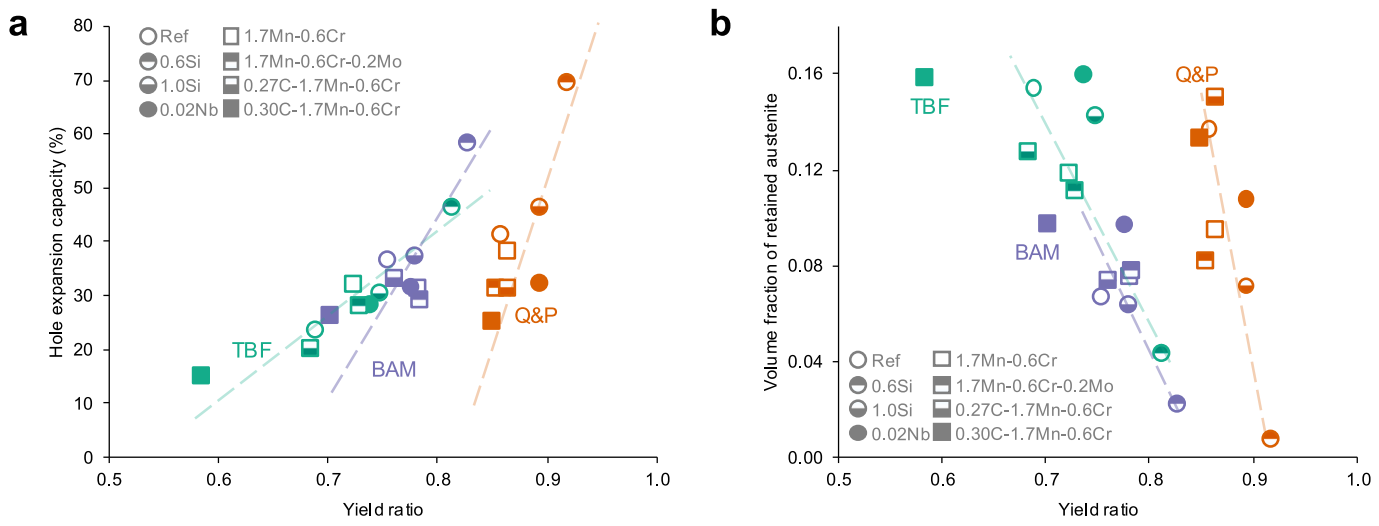

Fig. 9. Yield ratio plotted against (a) hole expansion capacity and (b) volume fraction of retained austenite. Shape of the markers indicates the chemical composition, color indicates the treatment, and dashed lines are the linear trends calculated separately for each group of samples with the same heat treatment. The isothermal holding time for the BAM samples was 600 s. (For interpretation of the references to color in this figure legend, the reader is referred to the Web version of this article.)

Carbon and silicon were the elements that influenced the mechanical properties the most. Fig. 10a and b show that both carbon and silicon increase the UTS while increasing (or maintaining) the total elongation. However, the trend is the opposite for the YS and the HEC, as shown in Fig. 10c and d. Both carbon and silicon decrease YS (or only slightly increase it, such as carbon in Q&P, Fig. 10d) and HEC. No specific trend was found for the other alloying elements.

The pronounced effect of silicon and carbon on the mechanical properties could be related to their higher influence on the fraction and stability of retained austenite as compared to the other alloying elements investigated in the present work. As shown in Fig. 8, the fraction retained austenite is positively correlated with the total elongation, but negatively correlated with the HEC. Silicon increases the fraction of retained austenite (Fig. 4) by inhibiting carbide formation [42], which in turn negatively affects the HEC. Retained austenite is less strong than bainite and martensite, and thus contributes little to the YS, which is possibly why increasing silicon content decreased YS. However, upon plastic deformation, the carbon-enriched retained austenite transforms into strong fresh martensite that increases the UTS. A similar mechanism might be operating for carbon. For instance, for TBF, increasing carbon also led to a higher fraction of retained austenite, UTS, and total elongation, and to a lower YS and HEC.

Despite the weak influence on the mechanical properties, substituting 0.6 wt.% Mn by 0.6 wt.% Cr refined the MA blocks (Fig. 3) due to a higher kinetics of bainite formation (Fig. 5). Even though bainite formation was faster in steel 1.7Mn-0.6Cr, no proeutectoid ferrite was found, neither in the microstructural characterization nor in the dilatometry curves, which indicates the steel has sufficient hardenability. The present finding that 0.6 wt.% Mn has the same effect on the hardenability as 0.6 wt.% Cr is consistent with the results presented by Grange [54].

The faster bainite kinetics while maintaining hardenability by the partial substitution of manganese for chromium can be explained in terms of driving force and diffusivity. In bainite formation, there is no diffusion of substitutional alloying elements [55]. Thus, substitutional alloying elements influence the kinetics of bainite formation mostly by their effect on the driving force. Fig. 11a shows that the partial substitution of manganese for chromium increases the driving force for bainite nucleation, which in turn accelerates bainite formation [56,57].

Conversely, there is significant diffusion of substitutional alloying elements during the formation of proeutectoid ferrite. Such elements can partition between austenite and ferrite and segregate to the interface. Hence, substitutional alloying elements influence the overall kinetics of ferrite formation by their effect not only on the driving force but on the average atomic mobility. Fig. 11a shows that the partial substitution of manganese for chromium increases the driving force for ferrite nucleation, which is expected to accelerate the formation of ferrite. However, the diffusion coefficient of the solute atoms in austenite and ferrite also heavily influences the kinetics of ferrite formation [58]. Fig. 11b shows that the diffusion coefficient of chromium is around one order of magnitude lower than that of manganese both in austenite and in ferrite. Thus, even though partially substituting manganese for chromium increases the driving force for ferrite formation, it decreases the rate at which solute atoms can be transferred across the moving ferrite-austenite interface. The overall effect of this substitution will depend on the balance between the effect of driving force and diffusion coefficient, as well as on the segregation of elements to the ferrite-austenite interface, which slows down the transformation because of the solute drag effect [59].

5. Conclusion

In this work we presented the design of a new 3rd gen AHSS that can be manufactured in existing continuous annealing lines for 1 mm thickness bare steel strips. Five different chemical compositions (Ref., 0.6Si, 1.0Si, 1.7Mn-0.6Cr, and 1.7Mn-0.6Cr-0.2Mo) met the requirements of steel grade CR1000Y1370UTS-CH – even delivering a surplus in total elongation – while showing a HEC value equal to or higher than 30%. This was achieved by balancing the chemical composition of steels to simultaneously have sufficient hardenability – meaning little to no formation of proeutectoid ferrite during cooling with rates typical of continuous annealing lines – and fast bainite kinetics. In the steels called BAM (bainite accelerated by martensite), the formation of a volume fraction of around 0.2 of prior martensite accelerated bainite formation and allowed an isothermal holding time of only 300 s. We also studied the effect of varying the content of selected alloying elements (C, Mn, Si, Cr, Mo, and Nb) and varying the heat treatment (BAM, TBF, and Q&P) on the microstructure and mechanical properties of the steels, and found that:

i) Bainite formation is significantly accelerated by fractions of prior martensite as low as 0.05. This pronounced acceleration effect at low fractions of martensite can be used to shorten the heat

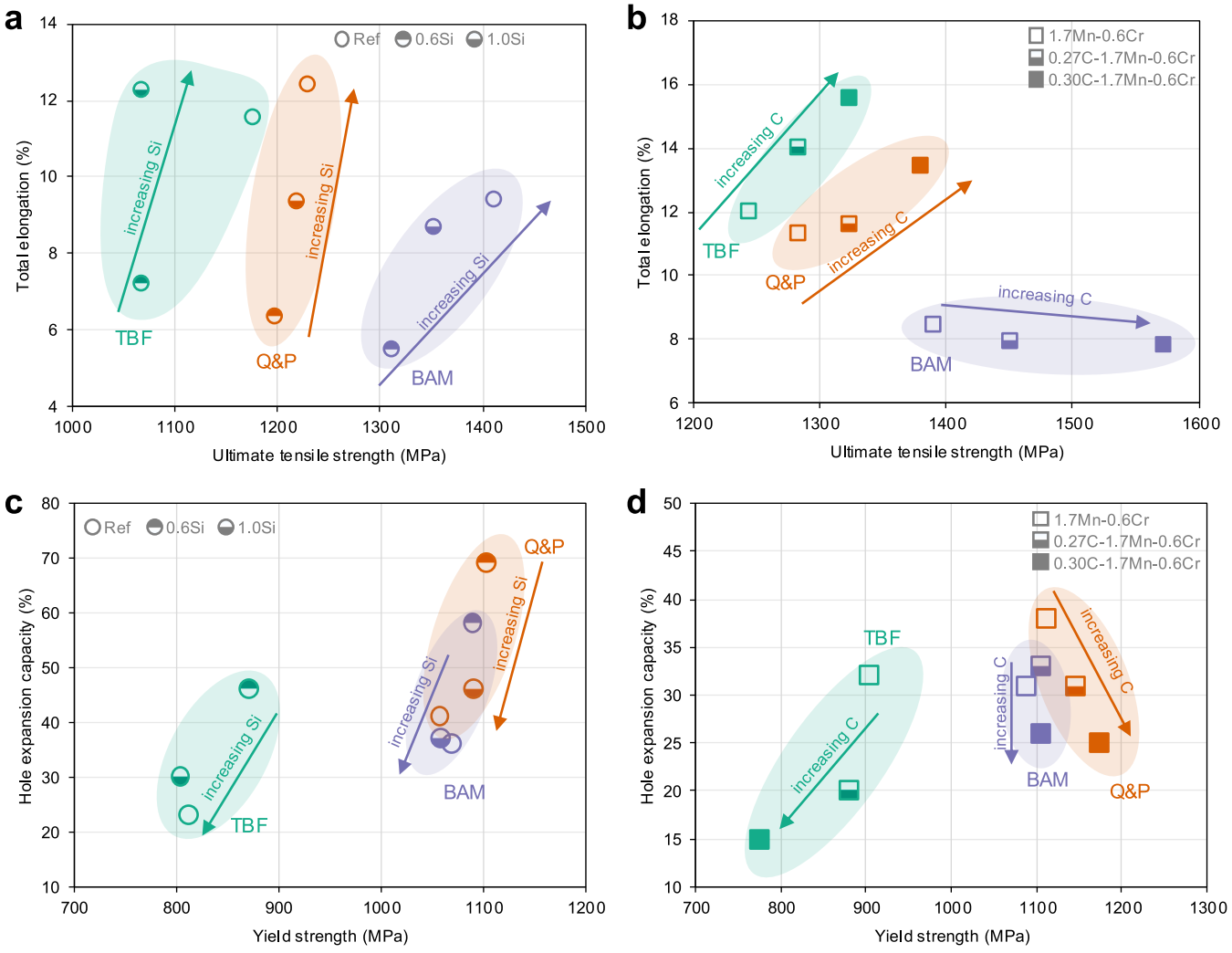

Fig. 10. Effect of (a,c) silicon and (b,d) carbon on the balance between (a,b) UTS and total elongation and (c,d) YS and HEC. Shape of the markers indicates the chemical composition, and the color indicates the heat treatment. The isothermal holding time for the BAM samples was 600 s. (For interpretation of the references to color in this figure legend, the reader is referred to the Web version of this article.)

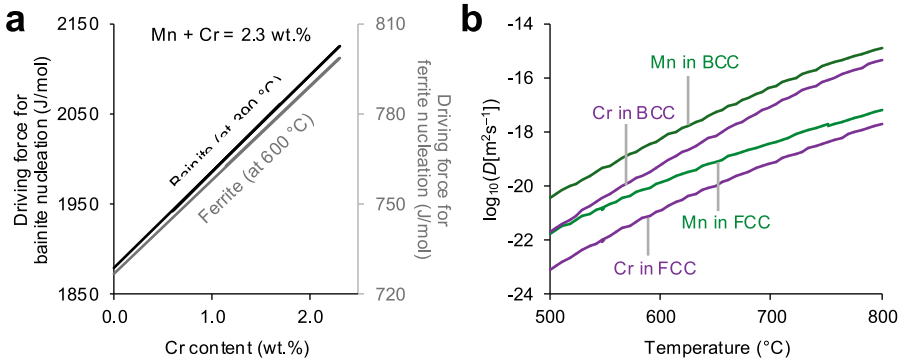

Fig. 11. (a) Driving force for bainite nucleation (values on left axis) at 390 °C and ferrite nucleation (values on right axis) at 600 °C as a function of the partial substitution of Mn for Cr in a Fe-0.24C-1.5Si-(2.3-x)Mn-xCr wt.% steel. (b) Log of the tracer diffusion coefficient, D, in m^2s^{-1} of Mn and Cr in ferrite (body-centered cubic, BCC) and austenite (face-centered cubic, FCC) as a function of temperature in a Fe-0.24C-1.5Si-1.7Mn-0.6Cr steel. All values were calculated using Thermo-Calc with databases TCFE12 and MOBFE7. The driving forces were calculated using the ferrite precipitation model within the steel model library of Thermo-Calc considering paraprecipitate for bainite and orthoprecipitate for ferrite.

treatment time of steels while maintaining a mostly bainitic microstructure.

ii) BAM heat treatment led to higher UTS but lower total elongation than TBF and Q&P because of its finer bainite laths and lower fraction of retained austenite. However, the lower fraction of retained austenite improved its local formability compared to TBF. This trend was verified for the steels and conditions tested here and might be different for different steel grades and ranges of temperature.

iii) Carbon and silicon are the elements that influence the mechanical properties the most because of their higher influence on the fraction and stability of retained austenite.

iv) The partial substitution of manganese for chromium accelerated bainite kinetics without any noticeable negative effect on hardenability. This partial substitution can be further investigated in future works to shorten even more the required time for bainite formation in 3rd gen AHSS.

CRediT authorship contribution statement

Daniel dos S. Avila: Writing – original draft, Visualization, Investigation, Formal analysis, Conceptualization. **Stefan M.C. van Bohemen:** Writing – review & editing, Resources, Methodology, Investigation, Funding acquisition, Formal analysis, Conceptualization. **Richard M. Huizenga:** Writing – review & editing, Resources, Methodology, Formal analysis, Data curation. **S. Erik Offerman:** Writing – review & editing, Supervision. **Maria J. Santofimia:** Writing – review & editing, Supervision, Methodology, Investigation, Funding acquisition, Formal analysis, Conceptualization.

Data availability

The data created for this work is available at: https://doi.org/10.4121/7a85f70f-9b8d-47b9-aba7-8fb74121a683 [60].

Funding

This project has received funding from the Research Fund for Coal and Steel under grant agreement number RFCS-2019-899251.

Declaration of competing interest

The authors declare that they have no known competing financial interests or personal relationships that could have appeared to influence the work reported in this paper.

Appendix A

Table A1
Mechanical properties of the steels heat treated in the CASim. The value presented is the mean of two tests, and the error is the average absolute deviation from the mean.

Heat treatment	Steel	YS (MPa)	UTS (MPa)	TE (%)	HEC (%)
BAM (600 s)	Ref	1069 ± 11	1413 ± 5	9.5 ± 1	36 ± 4
	0.6Si	1089 ± 8	1314 ± 15	5.5 ± 0.1	58 ± 2
	1.0Si	1059 ± 4	1355 ± 20	8.7 ± 0.5	37 ± 1
	0.02Nb	1063 ± 8	1366 ± 12	7.5 ± 0.2	31 ± 4
	1.7Mn-0.6Cr	1089 ± 2	1391 ± 2	8.5 ± 1.0	31 ± 1
	1.7Mn-0.6Cr-0.2Mo	1083 ± 6	1380 ± 2	10.4 ± 0.5	29 ± 4
	0.27C-1.7Mn-0.6Cr	1105 ± 15	1452 ± 17	7.9 ± 0.3	33 ± 4
	0.30C-1.7Mn-0.6Cr	1106 ± 9	1573 ± 15	7.8 ± 0.6	26 ± 3
BAM (300 s)	Ref	1026	1427	9.0	32
	0.6Si	1077	1390	8.1	40
	1.0Si	1018	1414	8.0	37
	0.02Nb	933	1394	9.6	25
	1.7Mn-0.6Cr	1039	1396	9.2	33
	1.7Mn-0.6Cr-0.2Mo	1018	1382	9.9	33
	0.27C-1.7Mn-0.6Cr	1103	1541	9.2	19
	0.30C-1.7Mn-0.6Cr	966	1669	8.5	19
TBF	Ref	813 ± 58	1177 ± 26	11.6 ± 1.8	24 ± 1
	0.6Si	870 ± 23	1069 ± 31	7.2 ± 1.3	46 ± 1
	1.0Si	803 ± 4	1071 ± 3	12.3 ± 0.3	30 ± 5
	0.02Nb	853 ± 8	1154 ± 1	12.2 ± 0.9	28 ± 3
	1.7Mn-0.6Cr	903 ± 13	1246 ± 2	12.1 ± 0.5	33 ± 10
	1.7Mn-0.6Cr-0.2Mo	938 ± 7	1278 ± 8	13.0 ± 0.7	28 ± 5
	0.27C-1.7Mn-0.6Cr	879 ± 20	1285 ± 2	14.0 ± 0.4	20 ± 1
	0.30C-1.7Mn-0.6Cr	778 ± 15	1325 ± 4	15.5 ± 0.3	16 ± 1
Q&P	Ref	1061 ± 20	1231 ± 9	12.4 ± 1.2	42 ± 10
	0.6Si	1108 ± 4	1205 ± 5	6.4 ± 0.7	70 ± 3
	1.0Si	1091 ± 22	1218 ± 13	9.3 ± 0.7	46 ± 2
	0.02Nb	1134 ± 15	1269 ± 9	11.3 ± 1.3	32 ± 1
	1.7Mn-0.6Cr	1112 ± 16	1286 ± 8	11.3 ± 0.1	38 ± 2
	1.7Mn-0.6Cr-0.2Mo	1107 ± 15	1297 ± 12	12.1 ± 0.2	31 ± 4
	0.27C-1.7Mn-0.6Cr	1145 ± 2	1326 ± 5	11.6 ± 0.1	31 ± 3
	0.30C-1.7Mn-0.6Cr	1167 ± 27	1371 ± 15	13.4 ± 0.5	26 ± 4

Data availability

The data has been uploaded to a repository and is cited in the article

References

[1] N. Fonstein, Advanced High Strength Sheet Steels: Physical Metallurgy, Design, Processing, and Properties, Springer International Publishing, 2015, https://doi.org/10.1007/978-3-319-19165-2.

[2] VDA 239-100 - Sheet Steel for Cold Forming (06/2016), 2016.

[3] C.C. Tasan, M. Diehl, D. Yan, M. Bechtold, F. Roters, L. Schemmann, C. Zheng, N. Peranio, D. Ponge, M. Koyama, K. Tsuzaki, D. Raabe, An overview of dual-phase steels: advances in microstructure-oriented processing and micromechanically guided design, Annu. Rev. Mater. Res. 45 (2015) 391–431, https://doi.org/10.1146/annurev-matsci-070214-021103.

[4] B.C. De Cooman, Structure–properties relationship in TRIP steels containing carbide-free bainite, Curr. Opin. Solid State Mater. Sci. 8 (2004) 285–303, https://doi.org/10.1016/j.cossms.2004.10.002.

[5] X. Li, A. Ramazani, U. Prahl, W. Bleck, Quantification of complex-phase steel microstructure by using combined EBSD and EPMA measurements, Mater. Char. 142 (2018) 179–186, https://doi.org/10.1016/j.matchar.2018.05.038.

[6] S. Allain, J.-P. Chateau, D. Dahmoun, O. Bouaziz, Modeling of mechanical twinning in a high manganese content austenitic steel, Mater. Sci. Eng., A 387–389 (2004) 272–276, https://doi.org/10.1016/j.msea.2004.05.038.

[7] K. Sugimoto, T. Iida, J. Sakaguchi, T. Kashima, Retained austenite characteristics and tensile properties in a TRIP type bainitic sheet steel, ISIJ Int. 40 (2000) 902–908, https://doi.org/10.2355/isijinternational.40.902.

[8] J. Speer, D.K. Matlock, B.C. De Cooman, J.G. Schroth, Carbon partitioning into austenite after martensite transformation, Acta Mater. 51 (2003) 2611–2622, https://doi.org/10.1016/S1359-6454(03)00059-4.

[9] Y.-K. Lee, J. Han, Current opinion in medium manganese steel, Mater. Sci. Technol. 31 (2015) 843–856, https://doi.org/10.1179/1743284714Y.0000000722.

[10] K. Hickey, Defining steels, AHSS guidelines. https://ahssinsights.org/metallurgy/defining-steels/, 2021. (Accessed 16 July 2024).

[11] K. Hickey, 3rd generation steels, AHSS guidelines. https://ahssinsights.org/metallurgy/steel-grades/3rd-generation-steels/, 2021. (Accessed 21 August 2024).

[12] W. Bleck, F. Brühl, Y. Ma, C. Sasse, Materials and processes for the third-generation advanced high-strength steels, Berg Huettenmaenn Monatsh 164 (2019) 466–474, https://doi.org/10.1007/s00501-019-00904-y.

[13] M.J. Santofimia, L. Zhao, R. Petrov, C. Kwakernaak, W.G. Sloof, J. Sietsma, Microstructural development during the quenching and partitioning process in a newly designed low-carbon steel, Acta Mater. 59 (2011) 6059–6068, https://doi.org/10.1016/j.actamat.2011.06.014.

[14] E.J. Seo, L. Cho, Y. Estrin, B.C. De Cooman, Microstructure-mechanical properties relationships for quenching and partitioning (Q&P) processed steel, Acta Mater. 113 (2016) 124–139, https://doi.org/10.1016/j.actamat.2016.04.048.

[15] E. De Moor, S. Lacroix, A.J. Clarke, J. Penning, J.G. Speer, Effect of retained austenite stabilized via quench and partitioning on the strain hardening of martensitic steels, Metall. Mater. Trans. A 39 (2008) 2586–2595, https://doi.org/10.1007/s11661-008-9609-z.

[16] X. Tan, Y. Xu, X. Yang, D. Wu, Microstructure–properties relationship in a one-step quenched and partitioned steel, Mater. Sci. Eng., A 589 (2014) 101–111, https://doi.org/10.1016/j.msea.2013.09.063.

[17] D. Sun, H. Wang, X. An, G. Wang, S. Huang, X. Huang, Quantitative evaluation of the contribution of carbide-free bainite, lath martensite, and retained austenite on the mechanical properties of C-Mn-Si high-strength steels, Mater. Char. 199 (2023) 112802, https://doi.org/10.1016/j.matchar.2023.112802.

[18] A. Navarro-López, J. Hidalgo, J. Sietsma, M.J. Santofimia, Influence of the prior athermal martensite on the mechanical response of advanced bainitic steel, Mater. Sci. Eng., A 735 (2018) 343–353, https://doi.org/10.1016/j.msea.2018.08.047.

[19] R. Hou, G. Xu, H. Hu, M. Zhou, Effects of Nb addition on transformation kinetics and microstructure properties in low-carbon bainitic steels, Metallogr. Microstruct. Anal. 6 (2017) 158–163, https://doi.org/10.1007/s13632-017-0345-x.

[20] L. Zhao, L. Qian, J. Meng, Q. Zhou, F. Zhang, Below-*Ms* austempering to obtain refined bainitic structure and enhanced mechanical properties in low-C high-Si/Al steels, Scr. Mater. 112 (2016) 96–100, https://doi.org/10.1016/j.scriptamat.2015.09.022.

[21] H. Hu, G. Xu, L. Wang, Z. Xue, Y. Zhang, G. Liu, The effects of Nb and Mo addition on transformation and properties in low carbon bainitic steels, Mater. Des. 84 (2015) 95–99, https://doi.org/10.1016/j.matdes.2015.06.133.

[22] E.P. Da Silva, D. De Knijf, W. Xu, C. Föjer, Y. Houbaert, J. Sietsma, R. Petrov, Isothermal transformations in advanced high strength steels below martensite start temperature, Mater. Sci. Technol. 31 (2015) 808–816, https://doi.org/10.1179/1743284714Y.0000000719.

[23] F.G. Caballero, S. Allain, J. Cornide, J.D. Puerta Velásquez, C. Garcia-Mateo, M. K. Miller, Design of cold rolled and continuous annealed carbide-free bainitic steels for automotive application, Mater. Des. 49 (2013) 667–680, https://doi.org/10.1016/j.matdes.2013.02.046.

[24] J.-C. Hell, M. Dehmas, S. Allain, J.M. Prado, A. Hazotte, J.-P. Chateau, Microstructure – properties relationships in carbide-free bainitic steels, ISIJ Int. 51 (2011) 1724–1732, https://doi.org/10.2355/isijinternational.51.1724.

[25] K. Sugimoto, M. Murata, S.-M. Song, Formability of Al–Nb bearing ultra high-strength TRIP-aided sheet steels with bainitic ferrite and/or martensite matrix, ISIJ Int. 50 (2010) 162–168, https://doi.org/10.2355/isijinternational.50.162.

[26] T. Hojo, K. Sugimoto, Y. Mukai, S. Ikeda, Effects of aluminum on delayed fracture properties of ultra high strength low alloy TRIP-aided steels, ISIJ Int. 48 (2008) 824–829, https://doi.org/10.2355/isijinternational.48.824.

[27] K. Sugimoto, M. Murata, T. Muramatsu, Y. Mukai, Formability of C–Si–Mn–Al–Nb–Mo ultra high-strength TRIP-aided sheet steels, ISIJ Int. 47 (2007) 1357–1362, https://doi.org/10.2355/isijinternational.47.1357.

[28] K.-I. Sugimoto, T. Muramatsu, S.-I. Hashimoto, Y. Mukai, Formability of Nb bearing ultra high-strength TRIP-aided sheet steels, J. Mater. Process. Technol. 177 (2006) 390–395, https://doi.org/10.1016/j.jmatprotec.2006.03.186.

[29] K. Sugimoto, J. Sakaguchi, T. Iida, T. Kashima, Stretch-flangeability of a high-strength TRIP type bainitic sheet steel, ISIJ Int. 40 (2000) 920–926, https://doi.org/10.2355/isijinternational.40.920.

[30] S. Ebner, C. Suppan, R. Schnitzer, C. Hofer, Microstructure and mechanical properties of a low C steel subjected to bainitic or quenching and partitioning heat treatments, Mater. Sci. Eng., A 735 (2018) 1–9, https://doi.org/10.1016/j.msea.2018.08.026.

[31] S.K. Paul, A critical review on hole expansion ratio, Materialia 9 (2020) 100566, https://doi.org/10.1016/j.mtla.2019.100566.

[32] S. Dhara, S.M.C. van Bohemen, M.J. Santofimia, Isothermal decomposition of austenite in presence of martensite in advanced high strength steels: a review, Mater. Today Commun. 33 (2022) 104567, https://doi.org/10.1016/j.mtcomm.2022.104567.

[33] Vda 239-100 – sheet steel for cold forming (05/2024). https://webshop.vda.de/VDA/vda-239-100-052024, 2024. (Accessed 20 July 2024).

[34] S.M.C. van Bohemen, J. Sietsma, Kinetics of martensite formation in plain carbon steels: critical assessment of possible influence of austenite grain boundaries and autocatalysis, Mater. Sci. Technol. 30 (2014) 1024–1033, https://doi.org/10.1179/1743284714Y.0000000532.

[35] S.M.C. van Bohemen, The nonlinear lattice expansion of iron alloys in the range 100–1600 K, Scr. Mater. 69 (2013) 315–318, https://doi.org/10.1016/j.scriptamat.2013.05.009.

[36] A. Navarro-López, J. Sietsma, M.J. Santofimia, Effect of prior athermal martensite on the isothermal transformation kinetics below ms in a low-C high-Si steel, Metall. Mater. Trans. A 47 (2016) 1028–1039, https://doi.org/10.1007/s11661-015-3285-6.

[37] C.F. Jatczak, Retained austenite and its measurement by X-ray diffraction, SAE Trans. 89 (1980) 1657–1676.

[38] P. Crowther, C.S. Daniel, xrdfit: a Python package for fitting synchrotron X-ray diffraction spectra, J. Open Source Softw. 5 (2020) 2381, https://doi.org/10.21105/joss.02381.

[39] D.N. Hanlon, S.M.C. van Bohemen, S. Celotto, Critical Assessment 10: tensile elongation of strong automotive steels as function of testpiece geometry, Mater. Sci. Technol. 31 (2015) 385–388, https://doi.org/10.1179/1743284714Y.0000000707.

[40] H.K.D.H. Bhadeshia, A rationalisation of shear transformations in steels, Acta Metall. 29 (1981) 1117–1130, https://doi.org/10.1016/0001-6160(81)90063-8.

[41] L. Leach, P. Kolmskog, L. Höglund, M. Hillert, A. Borgenstam, Critical driving forces for formation of bainite, Metall. Mater. Trans. A 49 (2018) 4509–4520, https://doi.org/10.1007/s11661-018-4819-5.

[42] S. Lin, A. Borgenstam, A. Stark, P. Hedström, Effect of Si on bainitic transformation kinetics in steels explained by carbon partitioning, carbide formation, dislocation densities, and thermodynamic conditions, Mater. Char. 185 (2022) 111774, https://doi.org/10.1016/j.matchar.2022.111774.

[43] S.M.C. van Bohemen, L. Morsdorf, Predicting the Ms temperature of steels with a thermodynamic based model including the effect of the prior austenite grain size, Acta Mater. 125 (2017) 401–415, https://doi.org/10.1016/j.actamat.2016.12.029.

[44] J.-O. Andersson, T. Helander, L. Höglund, P. Shi, B. Sundman, Thermo-Calc & DICTRA, computational tools for materials science, Calphad 26 (2002) 273–312, https://doi.org/10.1016/S0364-5916(02)00037-8.

[45] A. Suhane, D. Scheiber, V.I. Razumovskiy, M. Militzer, Atomistically informed phase field study of austenite grain growth, Comput. Mater. Sci. 228 (2023) 112300, https://doi.org/10.1016/j.commatsci.2023.112300.

[46] A. Navarro-López, J. Hidalgo, J. Sietsma, M.J. Santofimia, Characterization of bainitic/martensitic structures formed in isothermal treatments below the Ms temperature, Mater. Char. 128 (2017) 248–256, https://doi.org/10.1016/j.matchar.2017.04.007.

[47] L. Morsdorf, C.C. Tasan, D. Ponge, D. Raabe, 3D structural and atomic-scale analysis of lath martensite: effect of the transformation sequence, Acta Mater. 95 (2015) 366–377, https://doi.org/10.1016/j.actamat.2015.05.023.

[48] A. Creuziger, C.A. Calhoun, W.A. Poling, T. Gnäupel-Herold, Assessment of bias errors caused by texture and sampling methods in diffraction-based steel phase measurements, J. Appl. Crystallogr. 51 (2018) 720–731, https://doi.org/10.1107/S160057671800420X.

[49] P.J. Jacques, S. Allain, O. Bouaziz, A. De, A.-F. Gourgues, B.M. Hance, Y. Houbaert, J. Huang, A. Iza-Mendia, S.E. Kruger, M. Radu, L. Samek, J. Speer, L. Zhao, S. van der Zwaag, On measurement of retained austenite in multiphase TRIP steels — results of blind round robin test involving six different techniques, Mater. Sci. Technol. 25 (2009) 567–574, https://doi.org/10.1179/174328408X353723.

[50] S. Heibel, T. Dettinger, W. Nester, T. Clausmeyer, A.E. Tekkaya, Damage mechanisms and mechanical properties of high-strength multiphase steels, Materials 11 (2018) 761, https://doi.org/10.3390/ma11050761.

[51] S.V. Parker, Modelling of Phase Transformations in Hot-Rolled Steels, University of Cambridge, 1998. http://www.dspace.cam.ac.uk/handle/1810/221877. (Accessed 5 August 2024).

[52] c.H. Young, H.K.D.H. Bhadeshia, Strength of mixtures of bainite and martensite, Mater. Sci. Technol. 10 (1994) 209–214, https://doi.org/10.1179/mst.1994.10.3.209.
[53] J.H. Kim, E.J. Seo, M.-H. Kwon, S. Kang, B.C. De Cooman, Effect of quenching temperature on stretch flangeability of a medium Mn steel processed by quenching and partitioning, Mater. Sci. Eng., A 729 (2018) 276–284, https://doi.org/10.1016/j.msea.2018.05.083.
[54] R.A. Grange, Estimating the hardenability of carbon steels, Metall. Trans. A 4 (1973) 2231–2244, https://doi.org/10.1007/BF02669363.
[55] H.K.D.H. Bhadeshia, Bainite in Steels: Theory and Practice, third ed., third ed., CRC Press, London, 2015 https://doi.org/10.1201/9781315096674.
[56] D. dos S. Avila, S.E. Offerman, M.J. Santofimia, Modeling the effect of prior austenite grain size on bainite formation kinetics, Acta Mater. 266 (2024) 119656, https://doi.org/10.1016/j.actamat.2024.119656.
[57] L. Leach, J. Ågren, L. Höglund, A. Borgenstam, Diffusion-controlled lengthening rates of bainitic ferrite a part of the steel genome, Metall. Mater. Trans. A 50 (2019) 2613–2618, https://doi.org/10.1007/s11661-019-05208-x.
[58] H.S. Zurob, D. Panahi, C.R. Hutchinson, Y. Brechet, G.R. Purdy, Self-consistent model for planar ferrite growth in Fe-C-X alloys, Metall. Mater. Trans. A 44 (2013) 3456–3471, https://doi.org/10.1007/s11661-012-1479-8.
[59] I.-E. Benrabah, H.P. Van Landeghem, F. Bonnet, B. Denand, G. Geandier, A. Deschamps, Solute drag modeling for ferrite growth kinetics during precipitation experiments, Acta Mater. 221 (2021) 117364, https://doi.org/10.1016/j.actamat.2021.117364.
[60] D. dos Santos Avila, S. van Bohemen, R.M. Huizenga, E. Offerman, M.J. Santofimia, Dataset accompanying the article “Shortening the heat treatment of third generation advanced high strength steels by forming carbide free bainite in the presence of martensite,”. https://doi.org/10.4121/7A85F70F-9B8D-47B9-ABA7-8FB74121A683.V1, 2024.